Excerpt from the Proceedings of the 2011 COMSOL Conference in Boston

High Field Magnetic Diffusion into Nonlinear Ferrimagnetic Materials for Pulse Sharpening Applications

J.-W. Braxton Bragg[*1], James Dickens[1], Andreas Neuber[1], and Kevin Long[2]
[1]Center for Pulsed Power and Power Electronics, [2]Department of Mathematics and Statistics
Texas Tech University, Lubbock, TX, USA
*Corresponding author: braxton.bragg@ttu.edu

Abstract: Ferrimagnetic based, coaxial nonlinear transmission lines (NLTLs) provide a means to generate sub-nanosecond risetime pulses (from nanosecond input pulses) or megawatt level high power microwave oscillations, depending on the geometry, material, and external bias fields. The pulse sharpening observed in NLTLs is due to the nonlinear permeability sharply approaching unity with the application of a saturating pulse front. The nature of the pulse front is virtually unknown and almost always approximated as a linear ramp over time and spatially as cone-like with the apex at the inner conductor-ferrite boundary. Due to the fast risetimes involved, it is experimentally extremely difficult to directly observe magnetic diffusion into the material. Hence, this investigation uses the commercially available, finite element solver COMSOL to provide insight into pulse behavior. Maxwell's equations with nonlinear variables are solved for the ferrimagnetic material and pulse propagation is analyzed for axially symmetric (2D) coaxial line.

Keywords: Ferrimagnetic, nonlinear transmission line, pulse sharpening

1. Introduction

Nonlinear transmission lines (NLTLs) can be utilized as pulse sharpeners, triggers, or microwave sources [1], [2], [3]. In contrast to conventional high power microwave sources, which always require a high vacuum space for proper operation, the NLTL easily operates at ambient pressures or above. This specific type of NLTL consists of a coaxial geometry with toroidal ferrites snugly fit around the inner conductor. The nonlinearities inherent in the ferrimagnetic material allow for a compact pulse sharpener or microwave source.

The nonlinear permeability initially rests at a large value and upon application of an incident pulse of sufficient magnitude, the permeability sharply drops and approaches unity. This simple property results in hundreds of picoseconds risetime pulses formed from a few nanosecond risetime input.

The nature of the pulse sharpening line differs from the microwave generator in the sense that no external magnetic bias field is applied. With this in mind, pulse sharpening solely through ferrite saturation is considered.

Since little is known on mechanisms responsible for operation of NLTLs as HPM sources, modeling provides a measure of simulating various physics possibly responsible in hopes of building an optimal system. An efficient and accurate model would save time in the experimental setting allowing for slight tweaks of material properties, rather than designing and building new systems for material testing.

Experimentally, it has been observed that there exists a necessary risetime in order to generate microwaves and therefore a length of the NLTL is dedicated to only pulse sharpening. This preliminary study focuses on the possible achievable risetimes from ferrimagnetic saturation and includes comparisons to experimental results. Also, observations on the incident pulse front shape through propagation are made.

2. Model

2.1 COMSOL Model

The coaxial nature of the NLTL allows for a simple two-dimensional axisymmetric model; thereby significantly reducing model size and runtime. The model shown in Fig. 1 consists of input and output coaxial cables of dimensions matching RG-218 high voltage cable. The inner conductor of the RG-218 sections is copper with a polyethylene dielectric material and perfect electric conductor boundary condition in place of the outer conductor. The NLTL consists of a brass inner conductor, ferrimagnetic material

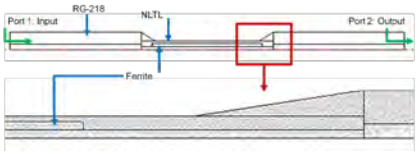

Figure 1. Model geometry including RG-218 coaxial cable, NLTL, input/output ports, and mesh.

snugly fit around the inner conductor, air dielectric, and perfect electric conductor boundary condition for outer conductor. The ferrite has a relative permittivity of 12, resistivity of 10^{-5} Ω·cm, and permeability as a function of magnetic field. The permeability is approximated by (1). The unsaturated and saturated relative permeability are denoted by μ_{us} and μ_s, respectively. The magnetic field at saturation is labeled B_{sat}.

$$\mu_r(B) = \mu_{us} - \mu_s \frac{1}{1+e^{-(B-B_{sat})*100}} \qquad (1)$$

The system dimensions are found in Table I and match the dimensions in the experimental setup.

The input and output ports (Port 1 and Port 2, respectively) are designated 50 Ω coaxial ports due to the overall system impedance of 50 Ω. Simulated waveforms are obtained through boundary integration variables with the radial component of the electric field as the expression.

Several waveforms are used as inputs in order to determine the effect of risetimes, pulse shapes, and incident magnitude on the overall pulse sharpening capabilities. The risetimes range from 1 – 8 ns with pulse shapes as linear ramp, smoothed Heaviside function with continuous second derivative (flc2hs), and critically damped *RLC* waveforms. The incident magnitudes are varied between 20 – 50 kV due to experimental design limitations.

Table I. Line and model dimensions

Item	Inner Diameter	Outer Diameter
RG-218 inner conductor (IC)	--	4.95 mm
RG-218 dielectric	4.95 mm	17 mm
NLTL IC	--	3 mm
Ferrite	3 mm	6 mm
NLTL OC	8 mm	12 mm

The simulations utilize the RF Module, Electromagnetic Waves, Hybrid-Mode Waves, Transient propagation mode. The subdomain equation is found in (2). Though experimental pulse widths range from 50 – 100 ns, most simulations are less than 15 ns for primary focus on the pulse front. The 25 ps time step is chosen to match the resolution capabilities of the oscilloscope used in experimental work.

$$\mu_0\sigma\frac{\partial \boldsymbol{A}}{\partial t} + \mu_0\frac{\partial \boldsymbol{A}}{\partial t}\left(\varepsilon_o\varepsilon_r\frac{\partial \boldsymbol{A}}{\partial t}\right) + \nabla\times\left(\frac{1}{\mu_r}(\nabla\times\boldsymbol{A})\right) = 0 \qquad (2)$$

2.2 Experimental setup

The experimental setup consists of a high voltage dc power supply, which charges a capacitor bank to a user controlled level. The capacitors are discharged through a pressurized, triggered spark gap. The pulse traverses commercially available RG-218 coaxial cable, enters the NLTL, and is terminated with a matched, 50 Ω resistive load.

The NLTL consists of a brass coaxial line with ferrimagnetic material along the inner conductor. The initial impedance of the line is O(1000), but due to the fast saturation of the ferrites, the line is designed to match 50 Ω upon saturation. Pressurized sulfur hexafluoride acts as the dielectric medium.

4. Results

Upon application of the high voltage pulse the relative permeability of the ferrimagnetic material is O(1000). As the voltage step increases, and consequently, the magnetic field increases, the permeability begins sharply dropping towards O(1) by means of (1). Due to the finite risetime of the incident pulse, the phase velocity seen with respect to radial distance is characterized by (3) where the inequality shows the initial, low voltage portion of the step is less than the final, high voltage portion of the step.

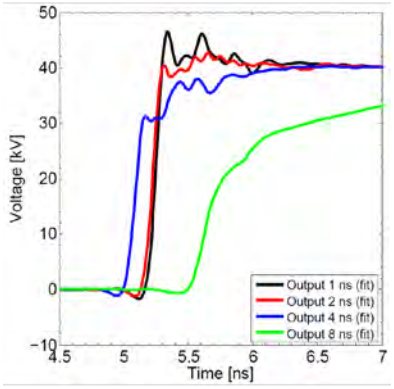

Figure 2. Outputs of NLTL model for incident risetimes of 1 ns, 2 ns, 4 ns, and 8 ns. The outputs shown are fitted with a smoothing function.

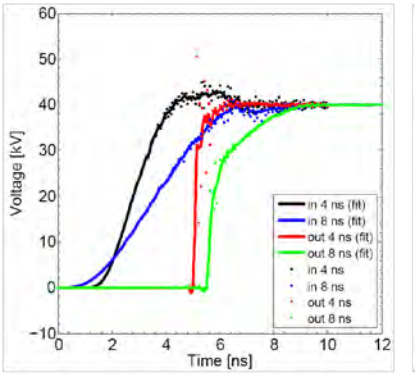

Figure 3. Input and output signals for 4 ns and 8 ns incident risetime. The solid lines are smooth fits of the numerical outputs (dotted lines).

$$v_{p,slow} = \frac{1}{\sqrt{C \cdot L(H_{10\%})}} < \frac{1}{\sqrt{C \cdot L(H_{90\%})}} = v_{p,fast} \quad (3)$$

The saturation and phase velocities that arise are a result of "catch-up" theory where the leading portion of the pulse front propagates with a slower phase velocity relative to the lagging portions, which allow the lagging portions to catch up. The result is an increased output phase velocity.

4.1 Output response to various inputs

The output waveforms have all been curve fit with a smoothing function to help alleviate numerical error. Error arises by way of reflection and are a result of not integrating dissipative factors into the model, namely in the relative permeability.

The NLTL pulse sharpening capabilities versus incident risetimes of 1 ns, 2 ns, 4 ns, and 8 ns are shown in Fig. 2. The 1 and 2 ns risetime signals produce near identical results with output risetimes on the order of 100 ps. The risetime of the 4 ns and 8 ns signals produce slower 10-90% risetimes, but still achieve significant pulse sharpening relative to the incident signal. The main difference between 8 ns risetime when compared to the other signals arises from the overall length of the NLTL. At saturation, the phase velocity is such that a signal will traverse the NLTL in approximately 6 ns. Consequently, an incident signal risetime exceeding the electrical length of the line will produce slower output risetimes. In Fig. 3, it is noted that the output signal begins following (in shape) the signal of the input at the calculated saturated electrical length of the NLTL.

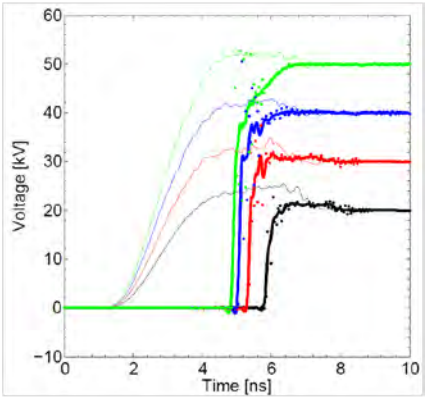

Figure 4. Input and output signals for varying incident pulse magnitude. The thin solid lines represent input signals; thick solid represent fitted output, and dotted represent numerical output.

The waveforms shown in Fig. 4 are the input and output waveforms for varying incident pulse magnitude. The bold, solid waveforms are the fitted simulation outputs, dotted waveforms are the raw simulation outputs, and the thin, solid waveforms are the simulated inputs. The inputs range from 20 – 50 kV with 4 ns risetime. Full saturation occurs with approximately 32 kV incident pulse magnitude. Consequently, the 20 kV and 30 kV signals do not reach complete saturation and therefore achieve slightly slower risetimes. The 40 kV and 50 kV signals achieve full saturation and upon surpassing the necessary saturation level, begin following the shape of incident waveform.

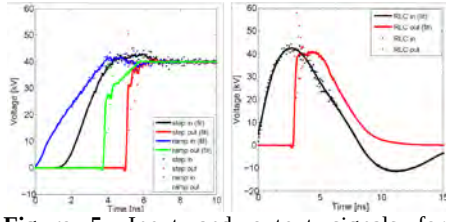

Figure 5. Input and output signals for varying incident pulse shape. The left set of waveforms contains figures for a smoothed Heaviside function (black, red) and a linear ramp (blue, green). The right figure is a critically damped *RLC* waveform.

Multiple waveform shapes were also simulated to determine the effects on output performance; see Fig. 5. The left graph in Fig. 5 has waveforms for the smoothed Heaviside function and a linear ramp function. Around the saturation point the output waveform for the linear ramp input moves to linear slope. The right graph is a critically damped *RLC* waveform and over the entire waveform most accurately resembles the experimental input pulse. The pulse front closely resembles the smoothed Heaviside, and as the pulse front is of highest concern, the smoothed Heaviside is used for the majority of simulations.

4.2 Field shape and permeability

In order to obtain an idea of the pulse front shape as it traverses the nonlinear medium, the magnetic flux density is measured versus the radial distance of the ferrimagnetic material as well as in the axial direction for several time steps; see Fig. 6. The waveforms in Fig. 6a are radial dependent magnetic flux density. The difference in field magnitude throughout the radial distance of the ferrite decreases as time progresses. The changing in pulse slope is indicative of pulse sharpening through saturation of the ferrite. Pulse steepening becomes more evident in Fig. 6b where the flux density is plotted versus the axial direction. As time increases the pulse front sharpens. Again, this is due to the larger magnetic field seen at the latter portion of the pulse front (high voltage side) producing a faster phase velocity; refer to (3).

Additionally, the relative permeability of the material is measured versus radial distance for all time steps in the simulation; see Fig. 7. The

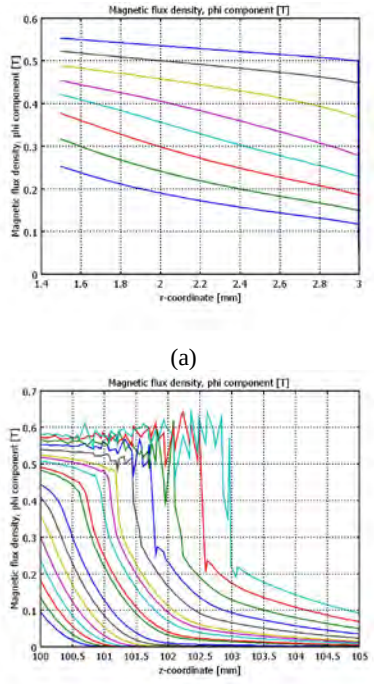

Figure 6. The magnetic flux densities versus radial (a) and axial (b) directions are shown at several time steps.

permeability begins falling at an exponential rate before becoming linear. This is believed to be a cause of the equation governing the permeability and can be assumed to be a first order accurate approximation due to the known nature of permeability versus magnetic field. Towards the later time steps, the signals become erratic and this is a result of induced reflections and lack of full dissipation characterization. The permeability eventually settles at the saturated value of 3.

4.3 Comparison to experimental data

Comparisons between experimental and simulated pulse sharpening for 30 kV, 40 kV, and 50 kV incident amplitudes are shown in Fig. 8. The risetime of the input signal is 4 ns for each voltage level. As the voltage level increases, the model more closely matches the experimental waveforms.

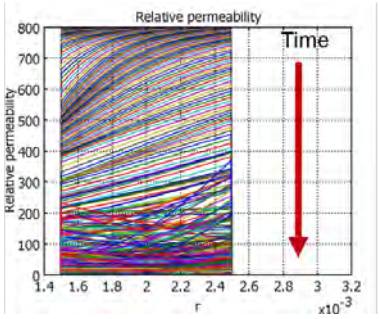

Figure 7. Relative permeability versus radial distance for several time steps.

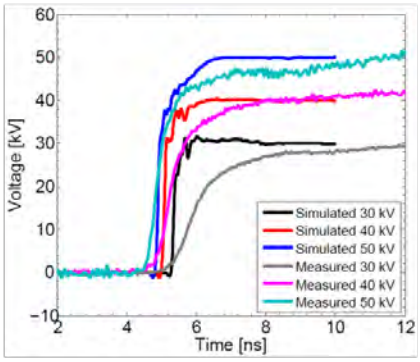

Figure 8. Comparison between simulated and experimental results for incident pulse magnitudes of 30 kV, 40 kV, and 50 kV.

One implication of the 30 kV comparison is the necessary integration of magnetic moment switching for an accurate simulation model. In the physical system, magnetic moments switch from a random orientation (or aligned with application of external magnetic bias) to a phi-directed position. This switching, which is not included in the model, accounts for some of the pulse sharpening. The 30 kV voltage level does not produce a field strong enough to switch the moments or saturate the material fast enough for the model to accurately match.

Additionally, the lack of material losses allows the model to produce faster output compared to experimental results. This fact is evident in the 40 kV shot, but not as much in the 50 kV shot. The experimental 50 kV shot produces a field strong enough to quickly switch the moments and saturate the material. The model also trends the incident wave after full saturation (see section 4.1). These effects result in an assumingly accurate model where inadequacies are hidden and would be missed if not for additional voltage levels.

These comparisons provide insight into additional factors that need be included in the model for accurate NLTL prediction.

7. Conclusions

The model presented to simulate pulse sharpening in NLTLs proves to be a good preliminary model and proof of concept of the pulse sharpening taking place during saturation of the nonlinear permeability. Comparisons with experimental data yield somewhat accurate results at the higher voltage levels with some deviations at the lower voltage. An idea of the affects of pulse risetime, shape, and magnitude has been explored as well as the nature of the permeability and propagating magnetic field.

Additional parameters that need to be integrated include full loss characterization in the ferrimagnetic material. In order to simulate the full NLTL supplementary physics need to be included, namely damped gyromagnetic precession for microwave generation.

8. References

1. N. Seddon, J. E. Dolan, and C. R. Spikings, “RF Pulse Formation in Nonlinear transmission Lines, *Proc. IEEE-ICOPS 34* (2007).

2. M. M. Turner, G. Branch, and P. W. Smith, “Methods of Theoretical Analysis and Computer Modeling of the Shaping of Electrical Pulses by Nonlinear Transmission Lines and Lumped-Element Delay Lines,” *IEEE Trans. Electron Devices*, **38**, pp. 810-816 (1991).

3. W. Sullivan III, “Investigation into Ferrite-Filled, Coaxial Nonlinear Transmission Lines for Pulse Sharpening”, Thesis for Master’s of Science, Texas Tech University (2009).